

Large-scale Vortices in Protoplanetary Disks: On the observability of possible early stages of planet formation

Sebastian Wolf

*California Institute of Technology, 1200 E California Blvd, Mail code 220-6, Pasadena, CA
91125, USA*

swolf@ipac.caltech.edu

H. Klahr¹

*Universität Tübingen, Institut für Astronomie und Astrophysik, Abt. Computational
Physics, Auf der Morgenstelle 10, D-72076 Tübingen, Germany*

hubert.klahr@uni-tuebingen.de

ABSTRACT

We investigate the possibility of mapping large-scale anti-cyclonic vortices, resulting from a global baroclinic instability, as pre-cursors of planet formation in proto-planetary disks with the planned Atacama Large Millimeter Array (ALMA). On the basis of three-dimensional radiative transfer simulations, images of a hydrodynamically calculated disk are derived which provide the basis for the simulation of ALMA. We find that ALMA will be able to trace the theoretically predicted large-scale anti-cyclonic vortex and will therefore allow testing of existing models of this very early stage of planet formation in circumstellar disks.

Subject headings: hydrodynamics, radiative transfer — techniques: interferometric — (stars:) circumstellar matter, planetary systems, pre-main sequence

1. Introduction

Klahr & Bodenheimer (2002) show that a global baroclinic instability represents a source for turbulence leading to angular momentum transport in Keplerian accretion disks with a

¹also at: UCO/Lick Observatory, University of California, Santa Cruz, CA 95060

radial gradient in entropy. Their hydrodynamical simulations show that this baroclinic flow is unstable and produces pressure waves, Rossby waves, and vortices in the $r - \phi$ plane of the disk. Most interestingly, these hyper-dens anti-cyclonic vortices form out of little background noise and become long-lasting features, which have been suggested to lead to the formation of planets (e.g. Adams & Watkins 1995). These pre-planetary matter concentrations have a surface density up to four times higher than the ambient medium. They furthermore concentrate dust in their centres, stressing their importance for the planetary formation process (e.g. Barge & Sommeria 1995).

2. Hydrodynamic and radiative transfer simulations

Using the code TRAMP (Klahr et al. 1999), we perform 2D hydrodynamic simulations of the evolution of the inner region (1–10 AU) of a circumstellar disk with an initial mass of $\approx 2 \times 10^{-3} M_{\odot}$. The comparison with previous models of circumstellar disks around T Tauri stars shows (see, e.g., Wood et al. 2002, Cotera et al. 2001) that this corresponds to a total disk mass on the order of $10^{-2} M_{\odot}$. As described by Klahr & Bodenheimer (2002) we treat the evolution of the vertically integrated density Σ and internal energy $\sim \Sigma T_{\text{cent}}$. The initial model had a slope in surface density of $R^{-0.75}$ and a temperature slope of $R^{-1.0}$ which represents a constant pressure scale height of $H/r = 0.055$. The vertically integrated pressure is then given by the ideal gas equation. Sources Q^+ for internal energy are the usual PdV -work as well as the dissipation of possible shocks via a simple von Neumann-Richtmyer viscosity (see Stone & Norman 1992). A sink for the internal energy is a black body cooling function $Q^- = aT_{\text{eff}}^4$ mimicking the effect of optically thick radiation in the disk and cooling with the effective (surface) temperature $T_{\text{eff}} = T_{\text{cent}}(4/3\tau)^{1/4}$ with the optical depth τ as a function of temperature and surface density. The simulation uses 128 cells in the azimuthal direction and 128 logarithmically distributed cells in the radial direction. The initial distribution was disturbed by a 0.1 percent perturbation in density and left to evolve freely afterwards under the influence of the global radial entropy gradient. After 10^4 yrs a huge anti-cyclonic hyper-dens vortex has formed (see Klahr & Bodenheimer 2002). Afterwards the 3D data was re-established by assuming a local vertical pressure equilibrium.

Based on the density and temperature distributions we performed radiative transfer simulations using the three-dimensional continuum radiative transfer code MC3D (Wolf 2002; see also Wolf et al. 1999, Wolf & Henning 2000). The goal of these simulations was to obtain images at frequencies of 345 GHz and 900 GHz. While the first frequency was chosen in order to allow comparison with former investigations focused mainly on this frequency, the second

frequency marks the planned upper limit of the frequency range to be covered by ALMA² and is of special importance for the observation of small spatial structures. The resulting images provide the basis for simulations of the continuum observations with ALMA discussed in §3.

Since we consider continuum observations at submillimeter wavelengths, the circumstellar dust is the dominant source of emission. The dust grains are assumed spherical, consisting of a mixture of 62.5 % astronomical silicate and 37.5 % graphite (optical data from Weingartner & Draine 2001³). For the graphite we adopt the usual “ $\frac{1}{3} - \frac{2}{3}$ ” approximation (Draine & Malhotra 1993). The size distribution $n(a)$ of the grains follows a power law, $n(a) \propto a^{-3.5}$, with grain radii in the range $0.005 \mu\text{m} \leq a \leq 1 \mu\text{m}$. The gas-to-dust mass ratio amounts to 100:1 in our simulations.

3. Simulations of observations with ALMA

For simulation of the observations with ALMA we use the simulator software published by Pety et al. (2001). Since the goal of the observation is to find small-scale structures in circumstellar disks, we consider the ALMA configuration with the longest baselines (max. baseline: ≈ 13 km) in which the 64 12m-antennas are distributed in rings. In accordance with the suggestions given by Pety et al. (2001), the following main types of errors are introduced in order to make the simulations realistic: (a) frequency-dependent receiver- and system temperatures as given by Guilloteau (2002), (b) random pointing error during the observation with a maximum value of of 0.6” in each direction, and (c) 30° phase noise. Further error sources, such as amplitude errors and “anomalous” refraction (due to the variation of the refractive index of the wet air along the line of sight) are considered as well. The observations are simulated for continuous observations centered on the meridian transit of the object. The object passes the meridian in zenith where an opacity of 0.15 is assumed. The bandwidth amounts to 8 GHz.

Fig. 1 shows simulated images of the undisturbed disk in comparison to the disk with the evolved baroclinic instability at 345 GHz and 900 GHz for object distances of 50 pc and 140 pc. The hyper-dens vortex is clearly visible even at the lower frequency. However, in the case of an assumed distance of 140 pc, the vortex causes a slight asymmetry in the reconstructed image only and could be hardly identified. Since several well-studied nearby

²See <http://www.arcetri.astro.it/science/ALMA/> for a compilation of ALMA related documents.

³See also <http://www.astro.princeton.edu/~draine>.

star-forming regions which can be observed from the prospective ALMA site are located at a distance between 140 pc and 200 pc, such as Taurus, Lupus, Ophiuchus, Corona Australis, and Chamaeleon, we concentrate on simulations at 900 GHz in the following. Furthermore, even more distant star-forming regions (e.g., in Aquila, Vulpecula, Vela, Perseus, Puppis, and Orion) are considered by comparison of simulated 900 GHz observations of the evolved disk seen under different inclinations in distances up to 300 pc in Fig. 2. While the main characteristics of the vortex (pre-planetary matter concentration), such as its spatial extent and brightness contrast to the surrounding medium clearly can be extracted from the images of objects at a distance of 140 pc, even the spiral pattern in the circumstellar disk (which is another, weaker feature of the disk in this evolutionary state) could be resolved in the case of a very close young stellar object such as TW Hya. At a distance of 300 pc the vortex is visible at low inclinations of the disk only, while it causes a slight asymmetry of the image at higher inclinations.

Finally, we consider possible observing strategies (selected objects vs. surveys) which mainly results in the question of required total integration time per object. In Fig. 3 images of the evolved disk seen face-on resulting from total integration times of 5 min to 8 h are shown. It turns out that exposure times of 5 min are sufficient to detect the vortex and to derive its roughly parameters. In order to map the spiral density structures in the case of an object at a distance of 50 pc, an integration time of 1-2 h is required. A longer exposure time does not significantly increase the information content of the reconstructed image. For objects in nearby star-forming regions (distance: 140 pc), a quick “snapshot” survey is sufficient since even much longer integration times will not allow derivation of further details of the turbulent structure of the disk.

4. Conclusions

We found that ALMA will be able to map the anti-cyclonic hyper-dens vortices from the global baroclinic instability representing an early stage of planet formation. In nearby star-forming regions, the main parameters of the predicted global baroclinic instability in proto-planetary disks can be derived within several minutes of integration time. For even closer objects (within a distance of about 50 pc) a detailed structure of the spiral density pattern will be possible. We want to stress that the largest planned baselines and high frequencies are required for these observations.

We wish to thank F. Gueth for many helpful suggestions concerning the ALMA simulator and L. Hillenbrand for careful reading of the manuscript. S. Wolf was supported through the

HST Grant GO 9160, and through the NASA grant NAG5-11645. H. Klahr was supported by the NASA grant NAG5-4610, the NSF grant AST 9987417, and by a special NASA astrophysics theory program which supports a joint Center for Star Formation Studies at NASA-Ames Research Center, UC Berkeley, and UC Santa Cruz.

REFERENCES

- Adams, F.C., & Watkins, R. 1995, *ApJ*, 451, 314
- Barge, P., & Sommeria, J. 1995, *A&A*, 295, L1
- Cotera, A.S., Whitney, B.A., Young, E., Wolf, M.J, Wood, K., et al., 2001, *ApJ*, 556, 958
- Draine, B.T., Lee, H.M., 1984, *ApJ*, 285, 89
- Draine, B.T., Malhotra, S., 1993, *ApJ*, 414, 632
- Guilloteau, S., 2002, ALMA Memo 393
- Klahr, H., Bodenheimer, P., 2002, *ApJ*, *subm.*
- Klahr, H., Henning, Th., Kley, W., 1999, *ApJ*, 514, 325
- Pety, J., Gueth F., Guilloteau S., 2001, ALMA Memo 398
- Stone, J.M., & Norman, M.L. 1992, *ApJS*, 80, 753
- Weingartner, J.C. & Draine, B.T., 2001, *ApJ*, 548, 296
- Wolf, S., 2002, *Comp. Phys. Comm.*, *in press*
- Wolf, S., Henning, Th., 2000, *Comp. Phys. Comm.* 132, 166
- Wolf, S., Henning, Th., Stecklum, B., 1999, *A&A*, 349, 839
- Wood, K., Wolff, M. J., Bjorkman, J.E., Whitney, B., 2002, *ApJ*, 564, 887

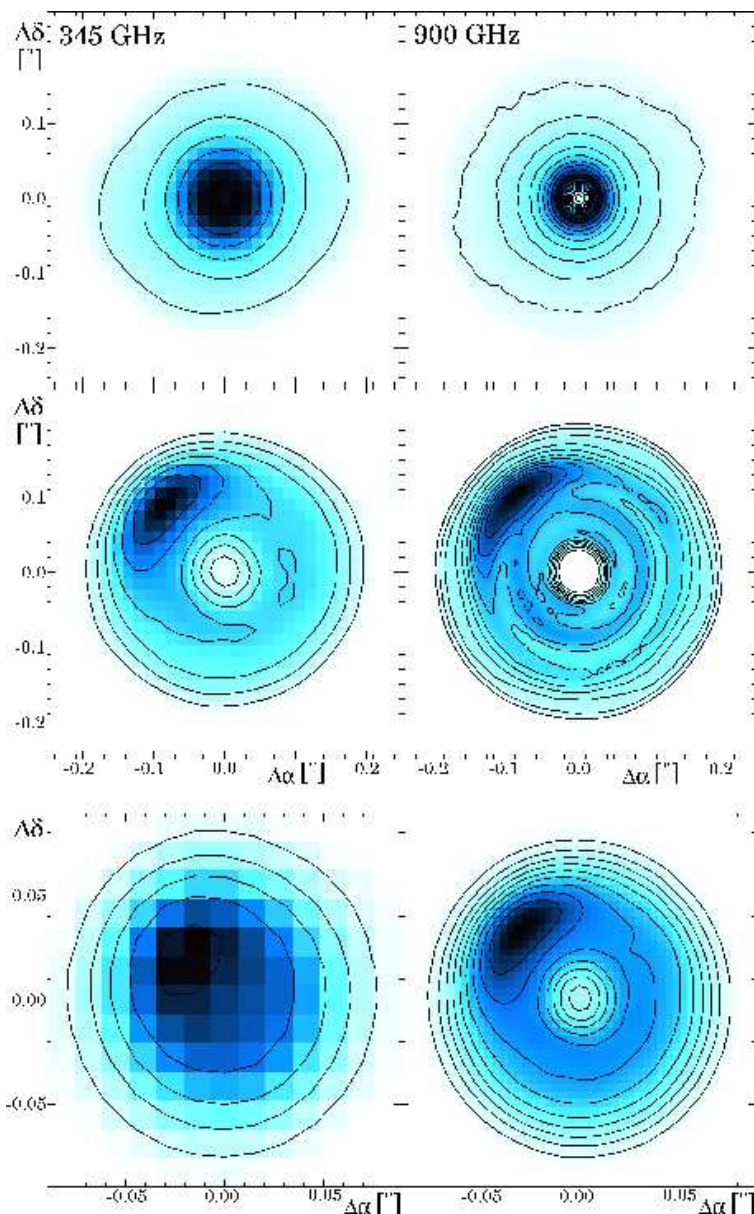


Fig. 1.— Reconstructed images of the disk seen face-on at $\nu=345$ GHz (left column) and 900 GHz (right column). *Upper row*: Undisturbed disk, distance 50 pc. *Middle/lower row*: Evolved disk with baroclinic instability, distance 50 pc/140 pc. The contour lines mark steps of 0.5 mJy/beam and 1.5 mJy/beam at $\nu=345$ GHz and $\nu=900$ GHz, respectively. Total integration time: 2 h.

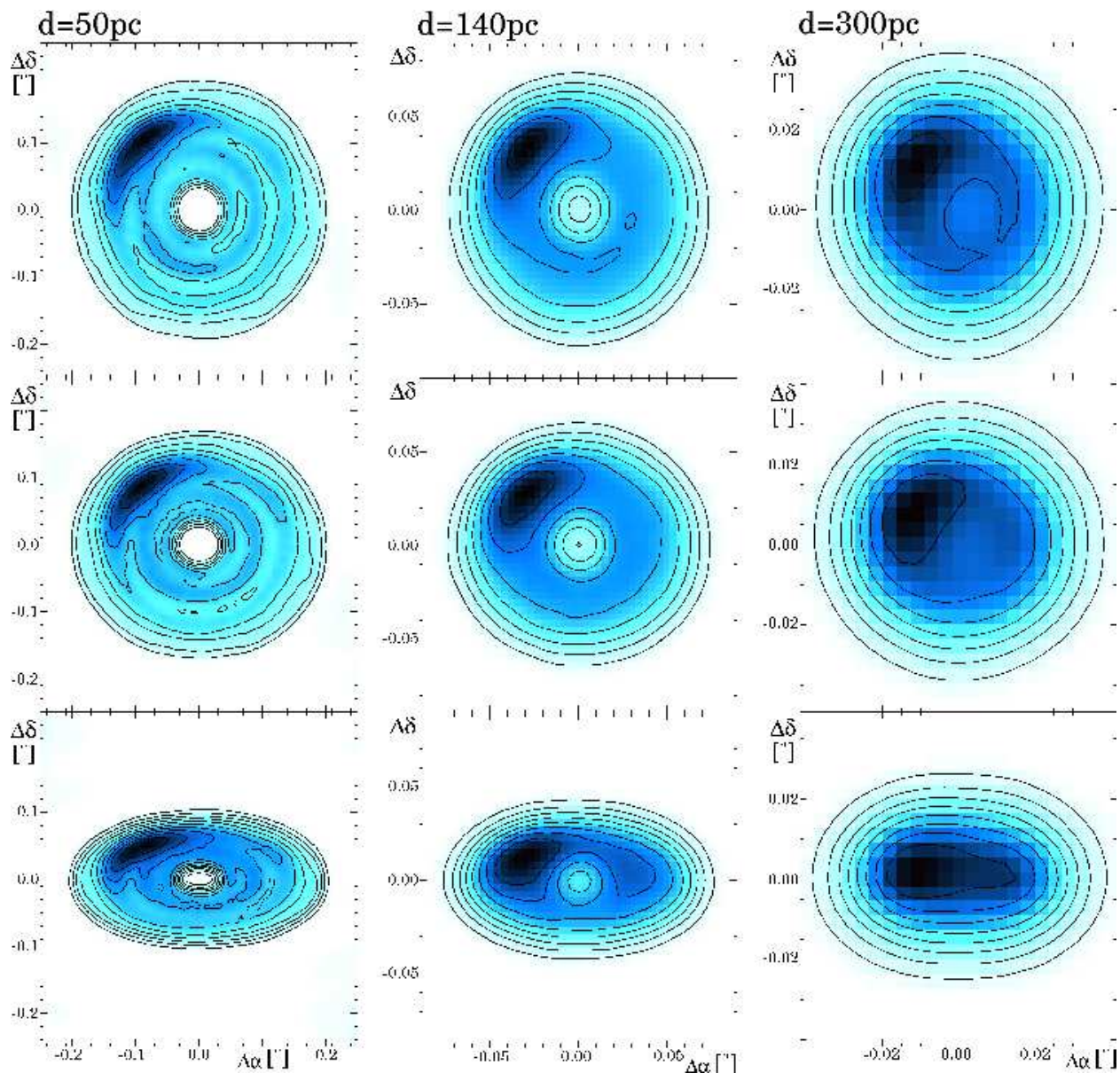


Fig. 2.— Reconstructed images of the evolved disk seen under inclinations of $i=0^\circ$ (face-on; upper row), 30° (middle row), and 60° (lower row). Distances of 50 pc, 140 pc, and 300 pc are considered. $\nu=900$ GHz; total integration time: 2 h. The contour lines mark steps of $2.0 \text{ mJy/beam}^{(1)}$ and $1.5 \text{ mJy/beam}^{(2)}$ in the case of $d=50 \text{ pc}^{(1)}$, $140 \text{ pc}^{(1)}$ and $300 \text{ pc}^{(2)}$, respectively.

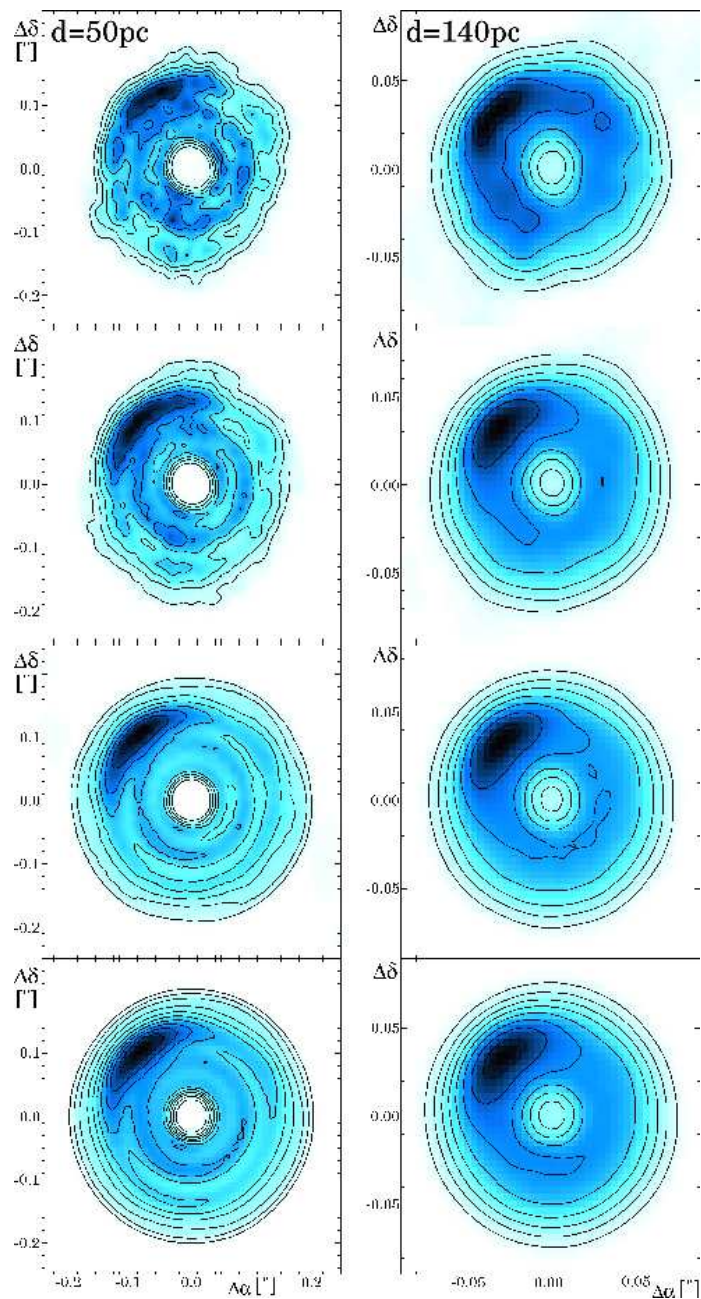


Fig. 3.— Reconstructed images of the evolved disk seen face-on in distances of 50 pc and 140 pc ($\nu=900$ GHz). Total integration times of 5 min, 24 min, 2 h and 8 h are assumed (from top to bottom). The contour lines mark steps of 2 mJy/beam.